Nuclear Science and Techniques (2026) 37:130
https://doi.org/10.1007/s41365-026-01951-0

Bayesian evaluation of photofission product yields of Th isotopic chains

Meng-Die Zhou[1,2] · Chun-Yuan Qiao[1] · Pu Jiao[1] · Hong-Wei Wang[2,3] · Hui-Ling Wei[4] · Gong-Tao Fan[2,3] · Jin-Gen Chen[5] · Chun-Wang Ma[6,1]

Received: 10 October 2025 / Revised: 22 December 2025 / Accepted: 5 January 2026 / Published online: 22 April 2026

Abstract
The fragment yields in photon-induced fission reactions of thorium (Th) isotopes are important for modern nuclear energy applications and for understanding the evolution of the nuclear structures of their isotopic chains. Bayesian neural network (BNN) models were constructed to describe the fragment yields in photonuclear fission reactions of thorium isotopes, ranging from ^{216}Th to ^{232}Th, especially those of ^{232}Th, at various incident photon energies. The predicted results of the optimized BNN models were in good agreement with the measured data for these reactions. The double-layer BNN models successfully illustrated the systematic transition from asymmetric to symmetric fission in thorium isotopes, including the associated odd-even effects, energy dependence, and leftward shift in mass yield distributions. The developed BNN models provide a new tool for predicting the fragment yields in thorium photonuclear fission reactions.

Keywords Photonuclear fission reaction · Thorium isotopes · ^{232}Th · Bayesian neural network · Total element yield · Mass chain yield · Odd-even staggering phenomenon

1 Introduction

The photon-induced nuclear fission (PNF) reaction of a heavy nucleus is a process in which high-energy photons interact with the nucleus, splitting it into two or more lighter hot fragments, followed by their decay processes that release neutrons, gamma rays, and energy [1, 2]. The mechanism of PNF differs from other particle-induced nuclear fissions because only an electromagnetic interaction exists between the photon and the nucleus [3–5], which can transfer a clear angular momentum and directly affect the distribution of the fission products, providing a clean probe for further research and understanding of the nuclear structure and nuclear reaction mechanism. The PNF process has important scientific and applied significance in many fields, such as nuclear physics research, energy development, nuclear medicine, and nuclear astrophysics [6, 7]. The PNF reaction also allows for a unique study of the interaction between the macroscopic and microscopic degrees of freedom in the nucleus. At low excitation energies, the reaction mechanism

This work was supported by the National Natural Science Foundation of China (Nos. 12375123 and 12247126), and the Natural Science Foundation of Henan Province (No. 242300421048).

✉ Hui-Ling Wei
htuwhling@126.com

✉ Gong-Tao Fan
fangt@sari.ac.cn

✉ Jin-Gen Chen
chenjingen@sinap.ac.cn

✉ Chun-Wang Ma
machunwang@126.com

1 School of Physics, Centre for Theoretical Physics, Henan Normal University, Xinxiang 453007, China

2 Shanghai Advanced Research Institute, Chinese Academy of Sciences, Shanghai 201204, China

3 University of Chinese Academy of Sciences, Beijing 101408, China

4 School of Optoelectronic, Henan Normal University, Xinxiang 453007, China

5 Shanghai Institute of Applied Physics, Chinese Academy of Sciences, Shanghai 201800, China

6 Institute of Nuclear Science and Technology, Henan Academy of Sciences, Zhengzhou 450046, China

is strongly influenced by the nuclear structure and the shell effect. The pairing effect plays an important role in the mass and nuclear charge distributions of fission fragments [8–10]. However, experimental data can only indirectly explain the influence of nuclear structure on the fission process. Additional data on PNF reactions are important for improving our understanding of this process [11, 12].

Machine learning techniques are algorithms for analyzing large amounts of data and uncovering patterns in complex high-dimensional data. By constructing sophisticated computational models, the nonlinear relationships inherent in the data can be effectively captured [13–15]. The Bayesian neural network (BNN) method uses Bayesian statistical methods to handle neural network models. Its core principle lies in assigning a prior probability distribution to the model parameters and then updating this prior through Bayes' theorem using observed data to obtain the posterior distribution of the parameters. Machine learning technologies have shown high quality in the prediction and analysis of atomic nuclear mass [16–19], nuclear physics [20, 21], photoneutron reactions [22], residual–nuclides cross sections in nuclear spallation [23–25] and projectile fragmentation [26–30] reactions. New theories based on machine learning have also been developed to describe the fission mechanism of heavy nuclides [31–33], such as extrapolating the nuclear mass, neutron-induced nuclear fission fragment yield, various nuclear structures, and observed quantities of reactions [34, 35]. Existing fission data are often incomplete and subject to large uncertainties. No study has yet applied Bayesian neural networks or similar frameworks to systematically predict both the charge and mass yields of photofission fragments across the entire thorium isotopic chain. Owing to the difficulties in describing fragment production in PNF reactions, BNN technology was systematically applied to construct models to evaluate and predict the fragment yields in PNF reactions of thorium isotopes for the first time. This approach was developed to meet the requirements of their important applications in modern nuclear reactors, nuclear medicine, and nuclear structure studies, as well as to evaluate the incomplete charge and mass distributions of the fragments. The excitation functions of the fragments of interest were also investigated.

The remainder of this paper is organized as follows: In Sect. 2, the method for building BNN models is described. In Sect. 3, the BNN evaluation of the total element yield and the mass chain yield of the PNF fragments are presented. A summary is provided in Sect. 4.

2 BNN models

The BNN can avoid the overfitting problem automatically by incorporating prior distributions, quantifying uncertainties in its predictions, and assessing correlations among model parameters [14, 21]. To construct a BNN model to reproduce and predict the cross section of fragments, the first step starts from the prior distribution of the model parameters by observing the given sample data $D = (x_1, t_1)...(x_N, t_N)$, x_n and t_n ($n = 1, 2,..., N$) are the input and output datasets, respectively. N denotes the total sample data. According to the Bayes theorem, the posterior probability distribution of the model parameters is obtained as follows

$$p(\theta \mid D) = \frac{p(D \mid \theta)p(\theta)}{p(D)}. \tag{1}$$

The model parameter θ is described probabilistically. $p(D \mid \theta)$ is the likelihood function of the argument model θ. $P(\theta)$ is the prior distribution, which is introduced for all possible values of θ. $P(D)$ is the normalized constant and represents the marginal density of the observed sample, which is defined as

$$p(D) = \int_\theta f(D \mid \theta) f(\theta) \mathrm{d}\theta. \tag{2}$$

For a regression task where the goal is to predict the noise vector of the target variable given an input vector, the likelihood function is typically defined to be a Gaussian distribution

$$p(D \mid \theta) = \exp\left(-\chi^2/2\right). \tag{3}$$

The objective function χ is defined as

$$\chi^2 = \sum_{n=1}^{N} \left(\frac{t_n - f(x;\theta)}{\Delta t_n} \right)^2, \tag{4}$$

where Δt_n is the noise error. The BNN model typically employs a multilayer perceptron (MLP) network, also known as a "backpropagation" or "feedforward" network. These networks consist of a set of input variables x_i, one or several hidden layers with different numbers of neurons, and one or more output variables $f_k(x;\theta)$. The functional equation of a typical MLP network with a single hidden layer is

$$f(x;\theta) = a + \sum_{j=1}^{H} b_j \tanh\left(c_j + \sum_{i=1}^{I} d_{ji} x_i \right), \tag{5}$$

where H is the number of hidden neurons in the hidden layer, and I is the number of input variables. $x = x_i$ is the dataset of the input variables. $\theta = \{a, b_j, c_j, d_{ji}\}$ defines the parameters of the MLP network equation corresponding to the biases and weights of the output layer, the biases, and the weights of the hidden layer, respectively. The total number of neurons is $1 + (2 + I) \times H$. In the BNN model, each output variable $f(x)$ is obtained by taking the weighted sum of the hidden unit values and adding the bias of the hidden layer. Each value of the hidden unit is calculated by taking the weighted sum of the input values and applying a nonlinear activation

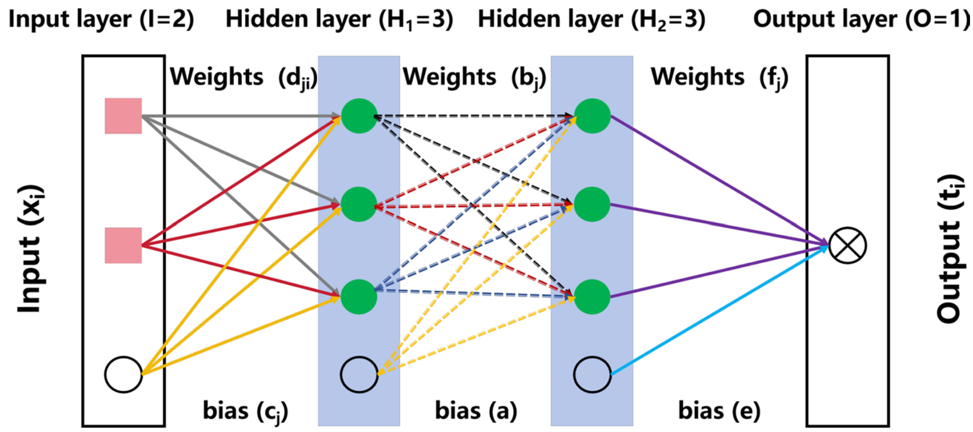

Fig. 1 (Color online) A schematic diagram of a neural network with a double hidden layers of 3–3 neurons ($H_1 = 3$, $H_2 = 3$) and two input variables ($I = 2$)

function. Figure 1 illustrates a schematic diagram of a typical neural network with double hidden layers of 3–3 neurons (H_1 =3, H_2 =3) and two input variables ($I = 2$).

Two independent BNN models were constructed to predict the yields of two different PNF fragment distributions: one for the charge yields (called BNN-CY) of PNF of thorium isotopes ($^{216\sim232}$Th) and another for the mass yields (called BNN-MY) of PNF fragments for ^{232}Th at different γ incident energies. All calculations in this study adopted a 10^5 sampling iteration of the BNN, and uncertainty quantification was presented with 80% confidence intervals (CIs). The optimal number of neurons in each layer was determined by systematically varying the number of neurons per layer and comparing the corresponding standard deviations χ_N^2 to determine the best configuration. The χ_N^2 is determined by

$$\chi_N^2 = \sum_i \left[t_i - f\left(x_i\right)\right]^2 / N. \tag{6}$$

3 Results and discussion

3.1 The fission mechanism of actinide elements

It is important to review the basic phenomena of the fragment yield distribution discovered in experiments before discussing the predicted results of the BNN models to better understand the evaluation of the fragment yields by BNN in γ-induced thorium fission reactions. In this subsection, we list the main experiments and their conclusions. The phenomenological Brosa model [36, 37], which is based on the mass distribution of fission products, postulates the existence of two asymmetric fission modes. The origin of these distinct asymmetric fission modes is attributable to the influence of fission barriers. The Brosa model further describes the broadening of fission observables through stochastic neck rupture, where longer necks correspond to a broader distribution. With the advancement of experimental research, three primary fission modes have been proposed for the nearly stable actinide region: two mass asymmetric modes, standard I (ST1) and standard II (ST2), and a super-long symmetric mode (SL) [38–40].

- ST1 is predominantly governed by doubly magic shell closure around ^{132}Sn, resulting in a nearly spherical heavy fragment.
- ST2 is characterized by the stabilization of the heavy fragment near $Z_f = 54$.
- SL exhibits a symmetric mass split, forming two fragments with comparable masses, both undergoing significant deformation.

Schmidt et al. [40, 41] investigated fission reactions of 70 short-lived radioactive isotopes in 2000, using the secondary beam facility at GSI Darmstadt. The primary beam of 1A GeV ^{238}U was irradiated on a beryllium target. The mass and charge of the produced fragments were analyzed using a Fragment Separator (FRS). These products were utilized as a secondary beam, which was excited by electromagnetic interaction with the secondary lead target, leading to fission of the nucleus within an excitation energy range of approximately 11 MeV, primarily by the giant dipole resonance. This study provides the first experimental characterization of the transition from asymmetric fission in actinides to symmetric fission in pre-actinides at the atomic level. Chatillon et al. [42] conducted a similar experiment at GSI in 2019, employing the R3B/SOFIA (Reactions with Relativistic Radioactive Beams/Studies on FIssion with Aladin) setup [43–45]. The mass and nuclear charge of the fission fragments were measured in coincidence with the total prompt neutron multiplicity, which provides evidence for the existence of a new compact symmetric fission mode in the light Th isotopic chain [46]. Based on the predictions of the BNN,

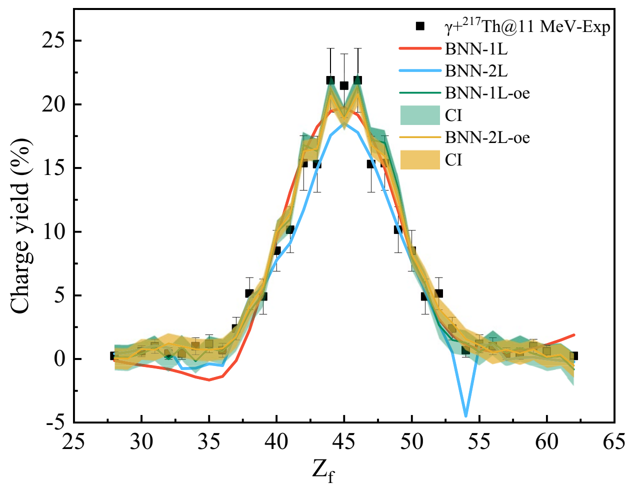

Fig. 2 (Color online) The photonuclear fission charge yields of $\gamma + {}^{217}$Th at excitation energy of 11 MeV predicted by BNN-CY model constructed based on the EXFOR data without ^{217}Th. Comparison of the charge yields for the ^{217}Th nuclide in this work (solid lines) and the experimental data from Ref. [42] (solid squares). The shadow region corresponds to the confidence interval (CI) at 80%

a detailed discussion of the photofission mechanism of the Th isotopes is presented in Sects. 3.2 and 3.3.

3.2 Total element yield of fission products

The BNN-CY model was constructed to predict the PNF fragment charge yields based on learning the experimental charge yield data in the EXFOR database, including 1437 experimental data points from the PNF products of 14 nuclides ($^{217\sim230}$Th). All measured data were obtained from Refs. [40, 42]. The input dataset of BNN-CY consists of $x_i = \{Z_{\mathrm{fi}}, Z_i, N_i, E_i\}$, which refers to the number of charges of the fission fragments, the number of charges and neutrons of the fission nucleus, and the excitation energy (E_i) of the compound nucleus, respectively. The output dataset t_i represents the charge yield of fission fragments. The fission charge yields of the compound nucleus ^{217}Th predicted by the BNN-CY model are illustrated in Fig. 2. For clarity, the prediction results of the neural network without the odd-even parameters only displayed the central values and did not include confidence intervals. The predictive results from single-layer neural networks, excluding odd-even parameters, demonstrate two notable anomalies: negative values emerge in the vicinity of the fission fragment charge $Z_{\mathrm{f}} =$ 35, while an abnormal upward tail becomes apparent for $Z_{\mathrm{f}} > 60$. Moreover, the double-layer neural network without odd-even parameters generated aberrant negative predictions near $Z_{\mathrm{f}} = 54$. The production of fission fragments with even numbers of protons is usually enhanced because the fully paired proton configuration tends to survive scission with a high probability. To describe the odd-even effect in the reaction system, we performed the methods described in Refs. [16, 32], an additional input $\delta = \pm 0.1$ was added to the BNN-CY learning collection to represent the number of atoms of even and odd fragments, respectively. The input parameter set becomes $x_i = \{Z_{\mathrm{fi}}, Z_i, A_i, E_i, \delta_i\}$. As can be seen in Fig. 2, BNN-CY evaluations without the odd-even parameter δ failed to capture the odd-even effect in the charge yield distribution of the PNF fragments, while the inclusion of the odd-even parameter δ allowed the BNN-CY to accurately reproduce the effect. Based on the values of χ_N^2 in Eq. (6), to screen the number of neurons in the hidden layers, a double-layer network with 30 neurons was adopted for the study.

Generally, a double-layer network significantly enhances the learning performance of data points owing to its larger number of connection parameters compared to a single-layer network, even when both have the same number of neurons. To verify this and better describe the odd-even effect in the reaction system, we conducted a more detailed comparison of the evaluation results of single-layer neural networks with odd-even parameters and those of double-layer neural networks with odd-even parameters. In particular, a single-layer network with 30 neurons and a double-layer network with 15–15 neurons were compared, with iterations of the BNN-CY sampling carried out 10^5. For both single-layer and double-layer networks, the standard deviations χ_N^2 obtained using Eq. (6) were 1.7×10^2 and 1.3×10^2, indicating similar uncertainties. In Figs. 3 and 4, as same as the double-layer network, the single-layer network can effectively reproduce the odd-even effect in the charge distribution of the fission fragments. However, the confidence interval of the double-layer network was slightly larger than that of the single-layer network.

Figure 3 presents a comparison between the results of the BNN-CY evaluation and the experimental charge yield data for the PNF fragments of the targets $^{217\sim229}$Th at an average excitation energy of 11 MeV, as reported by Schmidt et al. [40]. The BNN-CY results were in good agreement with the experimental data obtained. Notably, neural networks incorporating odd-even parameters successfully reproduced the characteristic odd-even staggering in the charge distribution of the reaction system. Furthermore, these calculations accurately captured the transition from asymmetric to symmetric fission in the PNF mechanism across the thorium isotopic chains. The number of peaks in the fission fragment charge distribution evolves with increasing neutron number of the target nuclei: single-peak distributions for neutron-deficient thorium targets transition through triple-peak patterns in intermediate-mass thorium nuclei, eventually becoming double-peak distributions for heavier thorium isotope targets. This systematic evolution demonstrates the strong dependence of the fission mechanisms on the number of neutrons along the Th isotopic chain. The experimental data on the

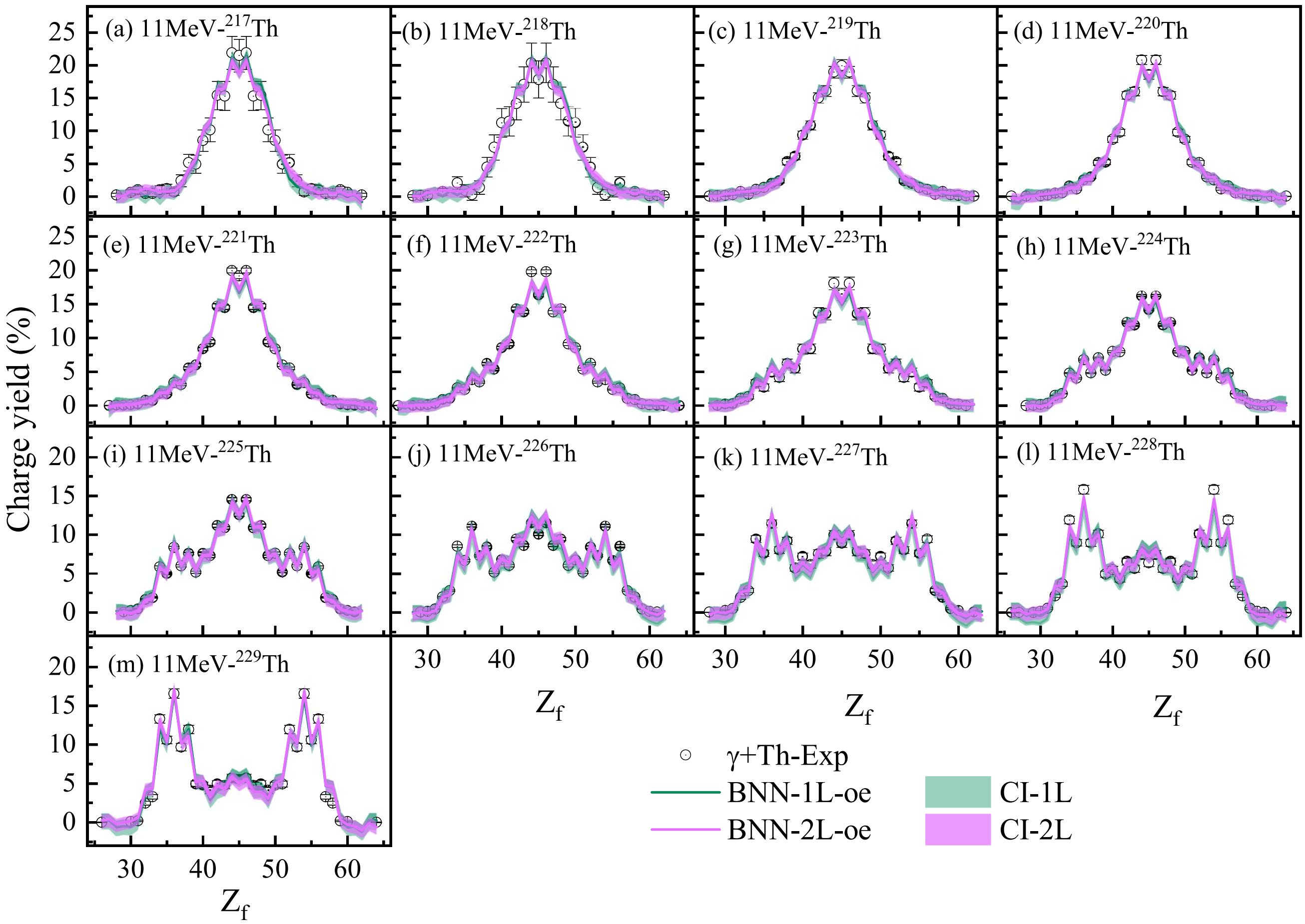

Fig. 3 (Color online) The charge yield distribution of fragments from γ-induced fission of thorium isotopes at excitation energy of 11 MeV. Comparison of one-layer (green lines) and two-layer (pink lines) BNN-CY learning results of the fragment charge yields from Ref. [40]. Open circles represent the experimental data. The shadow region corresponds to CI at 80%

charge yield of $^{221\sim230}$Th fission fragments at an average excitation energy of approximately 14 MeV, obtained by Chatillon et al. [42] are shown in Fig. 4 to exhibit a similar phenomenon.

The results predicted by the double-layer network with the smallest χ_N^2 value were selected for further evaluation and prediction, focusing on the charge yield values associated with the three prominent peaks observed in the fission fragment charge distribution across the Th isotopic chain. Fragments of $Z_\mathrm{f} = 36$ (Kr), 45 (Rh), and 54 (Xe) were analyzed because of their critical role in quantifying the competition between the symmetric and asymmetric fission modes. These yields serve as direct indicators of the evolving fission mechanism. Furthermore, the fission product ^{135}Xe has a substantial neutron absorption cross section, acting as a reactor "poison" that significantly reduces the operational power, and the evaluation of its production is of great importance. Figure 5 presents the evolution of the yields of the fission fragments for $Z_\mathrm{f} = 45$ (Rh) as a function of the target mass. The observed systematic decrease in the Rh fragment yields with increasing target neutron number clearly demonstrates the diminishing contribution of the symmetric fission channels. This trend culminates in near-zero fragment charge yields for $^{230\sim232}$Th, establishing asymmetric fission as the dominant mechanism in heavier thorium isotopes, whereas symmetric fission prevails in lighter Th isotopes. In particular, higher charge yields were observed at an excitation energy of 11 MeV in heavier Th isotopes than in the 13~15 MeV range. Figure 6 presents the evolution of the fission fragment yields for $Z_\mathrm{f} = 36$ (Kr) and 54 (Xe) as a function of the target mass number. The BNN-CY results successfully reproduced the symmetry characteristics of the charge yield distributions. The experimental data revealed a perfectly symmetric charge yield distribution, where the fragment Kr and Xe yields were identical, which was accurately reproduced by the BNN-CY predictions. Moreover, the charge yields of the fragments representing asymmetric fission mechanisms showed a systematic increase with the neutron number of the target nucleus, with a more pronounced

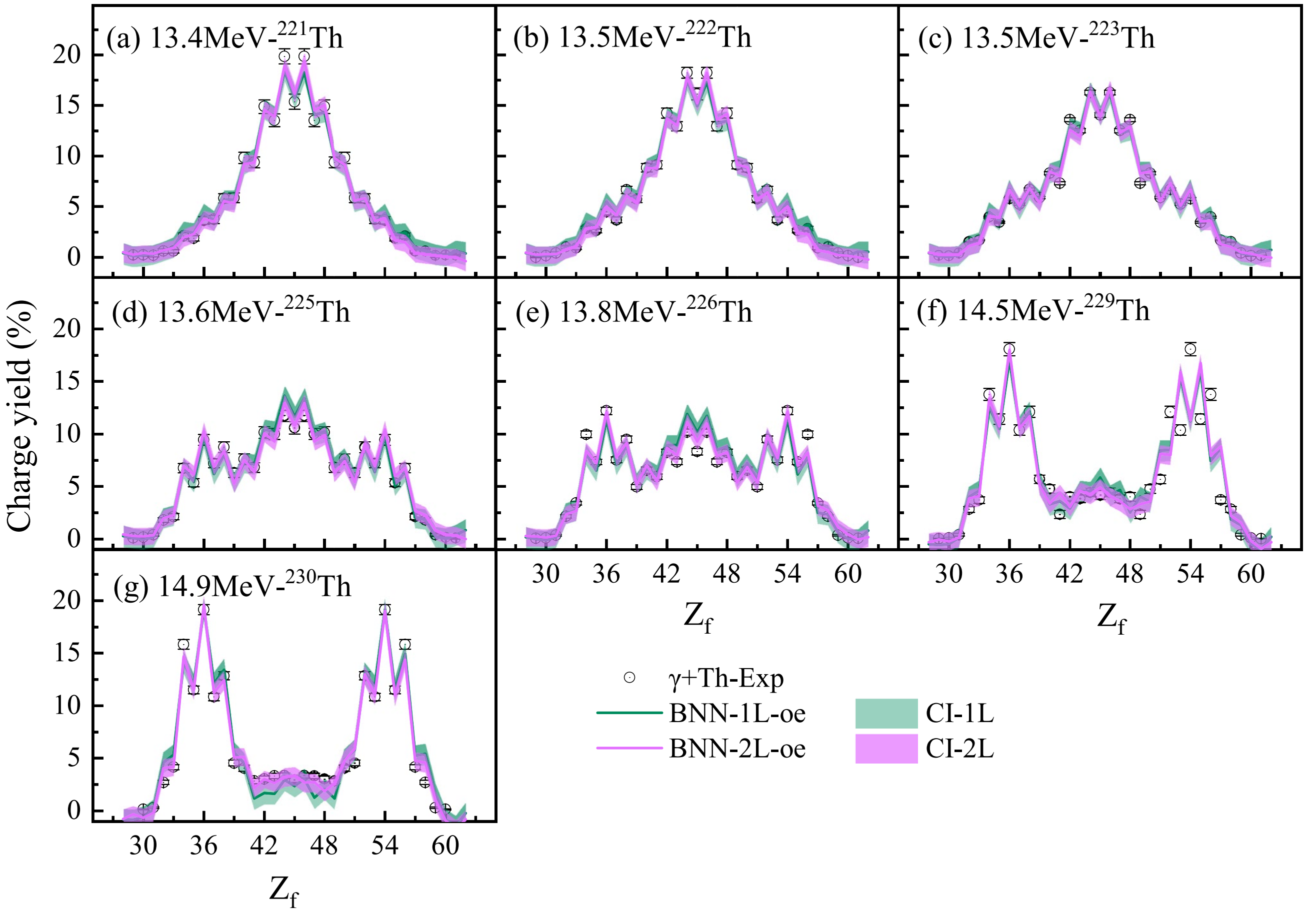

Fig. 4 (Color online) The charge yield distribution of fragments from γ-induced fission of thorium isotopes at different excitation energies. Comparison of one-layer (green lines) and two-layer (pink lines) BNN-CY learning results for the fragment charge yields from Ref. [42]. Open circles represent the experimental data. The shadow region corresponds to the CI at 80%

growth rate observed at an excitation energy of 14 MeV. These results provide clear evidence of the transition from symmetric fission in neutron-deficient thorium isotopes to asymmetric fission in heavier counterparts.

3.3 Mass chain yield distribution

The BNN-CY prediction in Sect. 3.2 indicates that the fission mechanism of ^{232}Th will be dominated by asymmetric fission. In this section, to explore the energy dependence of the mass yield distribution of fission fragments, the BNN-MY model was constructed based on learning experimental mass yield data in the EXFOR database, which includes 771 data points within an energy range of 8 ~ 80 MeV for the PNF products of ^{232}Th [47–54]. The mass yields of the fission fragments of ^{232}Th were measured by Naik et al. [49–54] using the activation method. To avoid systematic inconsistencies between different experimental datasets, which could lead to artificially widened confidence intervals in the model, we selected data exclusively from the same group (Naik et al.) for the training set, while using data from other groups for validation. The charge distribution exhibited a pronounced odd-even effect, which appeared to be obscured in the mass distribution. Consequently, there is no need to introduce the δ parameters as input corrections for the mass yield data. The network consists of a set of input variables $x_i = \{A_{fi}, Z_i, N_i, E_i\}$, which denote the mass number of the fission fragments, the number of charges and neutrons of the fission nucleus, and the incident γ energy (E_i), respectively. The output data t_i represent the mass yield of the fission fragments. We compared the single-layer network with 38 neurons and the double-layer network with 18–20 neurons, performing 10^5 BNN-MY sampling iterations. The standard deviations obtained for the single- and double-layer networks were 6.4×10^3 and 3.8×10^3, respectively. As shown in Fig. 7, the CI of the double-layer network is significantly narrower than that of the single-layer network. The double-layer network successfully reproduced the peak structures, whereas the results from the single-layer network appeared to be smoother. Based on these considerations, we

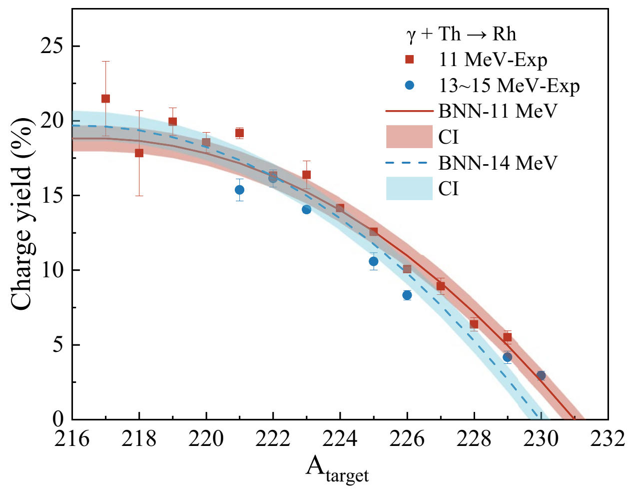

Fig. 5 (Color online) The BNN-CY predicted fission charge yields of $Z_f = 45$ of $\gamma + {}^{216\sim232}$Th at excitation energy of 11 MeV (full line) and 14 MeV (dotted line). Comparison of the charge yields for the Th isotopic chain in this study (lines) and the experimental data from Refs. [40, 42] (solid dots). The squares represent the experimental data of the charge yield at an excitation energy of 11 MeV, while the circular dots represent the experimental data of the charge yield in the excitation energy range of 13–15 MeV. The shadow region corresponds to the CI at 80%

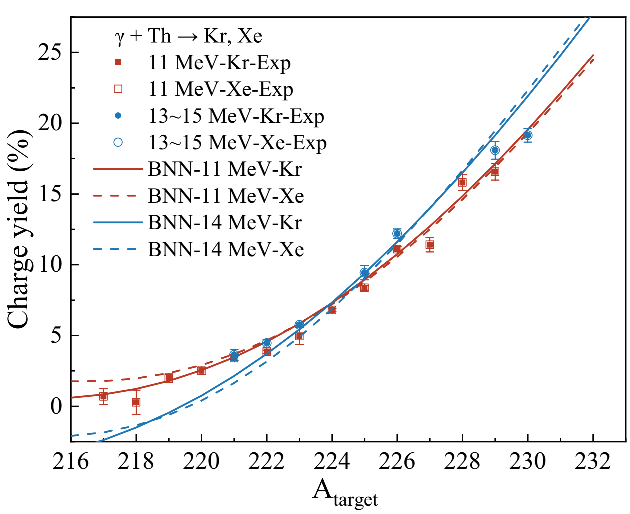

Fig. 6 (Color online) The BNN-CY predicted fission charge yields of $Z_f = 36$ and 54 of $\gamma + {}^{216\sim232}$Th at excitation energies of 11 MeV (red full line and dotted line) and 14 MeV (blue full line and dotted line). Comparison of the charge yields for the Th isotopic chain in this work (full lines) and the experimental data (solid dots) from Refs. [40, 42]. The squares represent the experimental data of the charge yield at an excitation energy of 11 MeV, while the circular dots represent the experimental data of the charge yield in the excitation energy range of 13–15 MeV. For the sake of clarity, the CIs are not shown in this BNN-CY results

selected a double-layer network as the more suitable model for further data evaluation in this study.

Figure 7 presents the BNN evaluation for regions with sparse experimental data points. In the mass region $A_f < 90$, experimental measurements are particularly scarce, demonstrating that the trained BNN model can predict the physical behaviors in regions where experimental data are currently scarce or inaccessible. The results show that the fission yield exhibits a monotonic increase with energy in the valley region (fragment mass number $A_f \approx 100 \sim 130$), whereas the twin peaks corresponding to the asymmetric fission modes diminish in prominence. In Fig. 8, $A_f = 91$ and 140 were selected for BNN prediction because the fragments with these mass numbers were, respectively, located in the light peak region and the heavy peak region of the asymmetric fission mode of ^{232}Th, and their yields were relatively high. Most importantly, these two fragments have sufficient experimental data that can be compared with the BNN prediction results. In general, the fragment yield of A_f=91, 140 representing asymmetric fission increases gradually within the incident γ energy range of $5 \sim 40$ MeV. However, when the γ energy exceeds 40 MeV, the yield decreases significantly rather than continuing to increase. In 2010, Demekhina et al. [38] compared the PNF fragment mass yields of ^{232}Th at γ energies of 50 and 3500 MeV. They observed that symmetric fission dominated as the energy increased, and its contribution increased by almost an order of magnitude. Moreover, owing to the additional emission of neutrons from the fission nucleus at higher excitation energies, the mass numbers of the fission fragments decrease, leading to a leftward shift in the mass yield distribution. Figure 9 displays the mass yield distributions evaluated by BNN-MY of ^{232}Th PNF fragments at incident γ energies of 8, 25, and 80 MeV. It can be seen that the yield of symmetric fission ($A_f = 100 \sim 130$) increases with energy. In contrast, the contributions of the light fragment peak ($A_f = 80 \sim 100$) and heavy fragment peak ($A_f = 130 \sim 150$) decrease progressively, which represents the symmetric fission mechanism. This suggests that with an increase in the excitation energy of the nucleus, particle evaporation (predominant neutron emission) occurs from the excited nucleus, which opens a new decay channel leading to the formation of neutron-deficient fission fragments (primarily through symmetric fission) [55, 56]. However, no obvious phenomenon of the light fragment peak moving toward a lower mass number was observed. This indicates that the PNF mechanism of ^{232}Th changes with the incident γ energy. In the low-energy region, the PNF mechanism of ^{232}Th mainly involves asymmetric fission, whereas in the high-energy region, it involves symmetric fission. Figure 10 shows the predictive capability of BNN-MY using a test set that excludes the PNF fragment mass yield data of ^{232} Th at the γ energies of 7.64 MeV and 17.5 MeV. A comparison between the predicted results and experimental measurements [57, 58] shows that BNN-MY can effectively predict the mass yields of PNF fragments

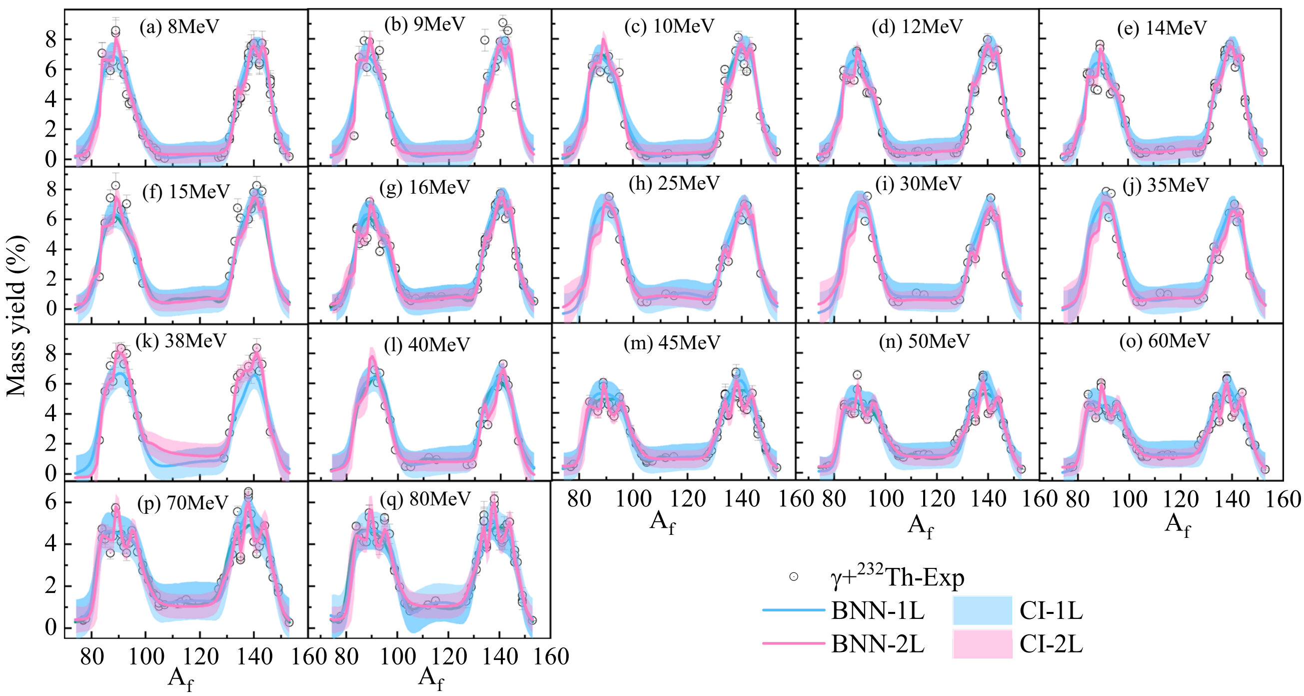

Fig. 7 (Color online) The mass yield distribution of fragments from γ-induced fission of ^{232}Th at different energies. Comparison of one-layer (blue lines) and two-layer (pink lines) BNN-MY learning results of fragment mass yields of γ+^{232}Th in γ energy range of 8–80 MeV from Naik et al. [49–54]. The shadow region corresponds to the CI at 80%

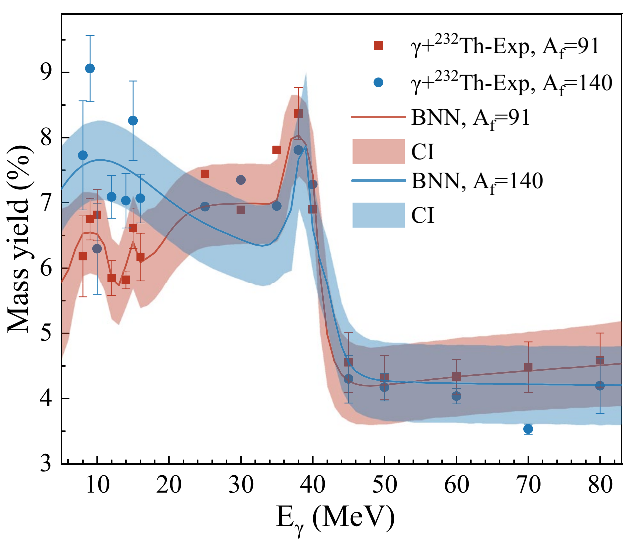

Fig. 8 (Color online) The excitation function of the mass yield of photonuclear fission fragments within the incident γ energy range of 5–80 MeV. The predicted results of BNN-MY (A_f = 91 as red line and A_f = 140 as blue line) are compared with the experimental data of the light asymmetric peak (A_f = 91 as square points) and the heavy asymmetric peak (A_f = 140 as circle points) [47–54]. The shadow region corresponds to the CI at 80%

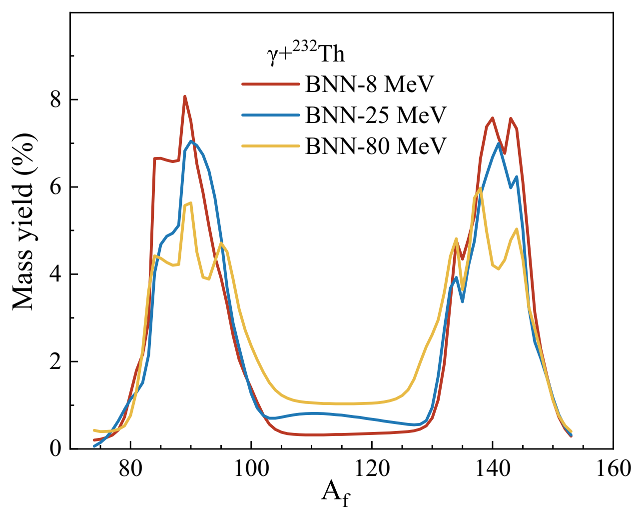

Fig. 9 (Color online) The BNN-MY predicted fission mass yield of γ+^{232}Th at γ energy of 8 MeV, 25 MeV, and 80 MeV. For clarity, the CIs are not shown in this BNN-MY results

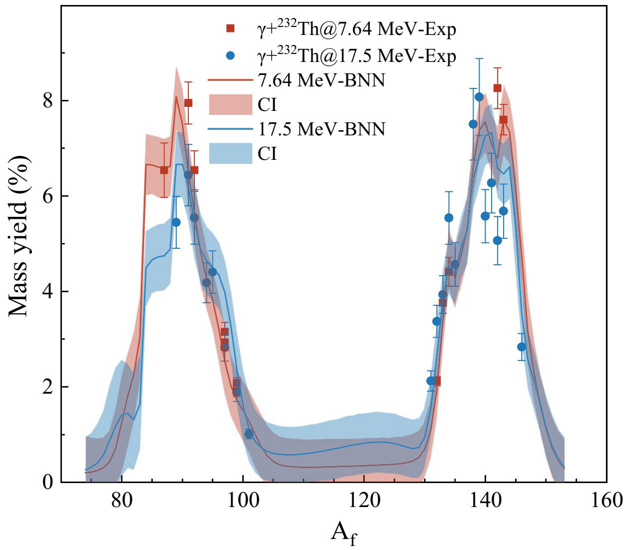

Fig. 10 (Color online) The BNN-MY predicted fission mass yield of $\gamma + {}^{232}$Th at γ energy of 7.64 MeV and 17.5 MeV, where the experimental data for these specific reactions were not included in the training dataset of BNN-MY. Comparison of the mass yields for the ^{232}Th nuclide in this work (solid lines) and the experimental data (solid points) from Ref. [57, 58]. The shadow region corresponds to the CI at 80%

for unstudied reactions, and the trained model successfully reproduces the results reported by other groups.

4 Summary

Nuclear fission is an extremely complex non-equilibrium quantum many-body dynamical process, and gaining deeper insights into fission remains a well-recognized challenge in nuclear physics. There remains a strong motivation to study nuclear fission, driven by expanding nuclear applications such as energy production and rare isotope generation, as well as in fundamental physics domains, including superheavy element synthesis and constraints on the *r*-process. This study presents the relationship between the yield and mass number of the target nucleus and the yield-energy correlation of the fission fragments of interest, which allows for an energy-dependent, two-dimensional distribution of the fission yields. The results reasonably reflect the evolution of the fission modes with increasing energy.

In the fission nuclei of lighter-mass regions, the charge yields of the PNF fragments tend to be symmetric. In the heavier-mass regions, the charge yields began to exhibit asymmetric components that gradually dominated, most notably in the isotopes of Th and Pa. The number of protons in the PNF fragments directly carries information about the scission. Experimentally, it has been observed that the production of PNF fragments with even proton numbers is typically enhanced, which is one of the most prominent features of fission fragment yields. To describe the odd-even effect in the reaction system, we added an additional input $\delta = \pm 0.1$ in the BNN-CY learning collection to represent the number of atoms in even and odd fragments, respectively. The uncertainty decreases after adding the odd-even effect, reflected in the PNF fragments charge distribution of the BNN-CY model, and also showed a regular transition from symmetric fission of the lighter Th isotopes to asymmetric fission of the heavier Th isotopes. The fission mechanism of the fissile nuclei evolves with the excitation energy of the reaction system. The mass distribution of PNF fragments predicted by the BNN-MY model indicates that asymmetric fission prevails at low excitation energies, whereas symmetric fission is the dominant mode at higher excitation energies. For ^{232}Th, asymmetric fission dominated at incident γ energies below 40 MeV, whereas the contribution of symmetric fission gradually increased at energies above 40 MeV. Furthermore, no leftward shift in the fragment mass distribution was observed within the γ energy range of several tens of MeV.

The BNN is a powerful and reliable tool for predicting the photofission fragment yields. It has successfully revealed the evolution of fission mechanisms and the associated odd-even effects, providing critical theoretical support for nuclear databases and reactor design. Currently, numerous facilities have begun to conduct research on PNF reactions, such as the high intensity γ-ray Source (HIγS) [59–61], GSI [43, 62], and the extreme light infrastructure nuclear physics (ELI-NP) [63–65]. Building upon the theoretical work presented in this study, future photofission experiments could be conducted using laser Compton scattering (LCS) γ rays at the Shanghai Laser Electron Gamma Source (SLEGS) at the Shanghai Synchrotron Radiation Facility (SSRF), which provides monoenergetic γ beams from 0.25 to 21.7 MeV [66, 67].

Author Contributions All authors contributed to the study conception and design. Material preparation, data collection and analysis were performed by Meng-Die Zhou, Chun-Yuan Qiao and Chun-Wang Ma. The first draft of the manuscript was written by Meng-Die Zhou and all authors commented on previous versions of the manuscript. All authors read and approved the final manuscript.

Data Availability The data that support the findings of this study are openly available in Science Data Bank at https://www.doi.org/10.57760/sciencedb.j00186.00990 and https://cstr.cn/31253.11.sciencedb.j00186.00990.

Declarations

Conflict of interest Chun-Wang Ma is an editorial board member for Nuclear Science and Techniques and was not involved in the editorial review, or the decision to publish this article. All authors declare that there are no conflict of interest.

References

1. A. Zilges, D.L. Balabanski, J. Isaak et al., Photonuclear reactions-from basic research to applications. Prog. Part. Nucl. Phys. **122**, 103903 (2022). https://www.sciencedirect.com/science/article/pii/S0146641021000624
2. H.L. Wei, M.D. Zhou, P. Jiao et al., SPAGINS: semiempirical parameterization for fragments in gamma-induced nuclear spallation. Nucl. Sci. Tech. **34**, 190 (2023). https://doi.org/10.1007/s41365-023-01342-9
3. M. Bender, R. Bernard, G. Bertsch et al., Future of nuclear fission theory. J. Phys. G Nucl. Part. Phys.**47**,113002 (2020).https://doi.org/10.1088/1361-6471/abab4f
4. D.L. Balabanski, P. Constantin, 80 years of experimental photofission research. Eur. Phys. J. A **60**, 39 (2024). https://doi.org/10.1140/epja/s10050-024-01264-z
5. M.D. Zhou, Z.R. Hao, Q.K. Sun et al., Measurement of ^{59}Co(γ, n)^{58}Co using a new flat-efficiency neutron detector at the Shanghai Laser Electron Gamma Source. Phys. Rev. C **111**, 054612 (2025). https://doi.org/10.1103/PhysRevC.111.054612
6. H.X. Zhang, T.R. Yeh, H. Lancman, Intermediate structure in the photofission cross section of ^{232}Th. Phys. Rev. Lett. **53**, 34 (1984). https://doi.org/10.1103/PhysRevLett.53.34
7. H.X. Zhang, T.R. Yeh, H. Lancman, Photofission cross section of ^{232}Th. Phys. Rev. C **34**, 1397 (1986). https://doi.org/10.1103/PhysRevC.34.1397
8. J.A. Sheikh, W. Nazarewicz, J.C. Pei, Systematic study of fission barriers of excited superheavy nuclei. Phys. Rev. C **80**, 011302(R) (2009). https://doi.org/10.1103/PhysRevC.80.011302
9. J.A. Silano, H.J. Karwowski, Near-barrier photofission in ^{232}Th and ^{238}U. Phys. Rev. C **98**, 054609 (2018). https://doi.org/10.1103/PhysRevC.98.054609
10. M.L. Yoneama, E. Jacobs, J.D.T. Arruda-Neto et al., Study of the ^{232}Th fission barrier by electron-induced fission. Nucl. Phys. A **604**, 3 (1996). https://doi.org/10.1016/0375-9474(96)00159-5
11. G.L. Wang, H.Y. Lan, X.M. Shi et al., A general framework for describing photofission observables of actinides at an average excitation energy below 30 MeV. Chin. Phys. C **46**, 084102 (2022). https://doi.org/10.1088/1674-1137/ac6abc. https://iopscience.iop.org/article/10.1088/1674-1137/ac6abc
12. X.M. Shi, G.L. Wang, K.J. Luo et al., Geant4 development for actinides photofission simulation. Nucl. Instrum. Meth. A **1062**, 169222 (2024). https://doi.org/10.1016/j.nima.2024.169222
13. H.F. Zhang, L.H. Wang, J.P. Yin et al., Performance of the Levenberg-Marquardt neural network approach in nuclear mass prediction. J. Phys. G Nucl. Part. Phys. **44**, 045110 (2017). https://doi.org/10.1088/1361-6471/aa5d78. https://iopscience.iop.org/article/10.1088/1361-6471/aa5d78
14. A. Boehnlein, M. Diefenthaler, N. Sato et al., Colloquium: machine learning in nuclear. Phys. Rev. Mod. Phys. **94**, 031003 (2022). https://doi.org/10.1103/RevModPhys.94.031003
15. P. Vicente-Valdez, L. Bernstein, M. Fratoni, Nuclear data evaluation augmented by machine learning. Ann. Nucl. Energy **163**, 108596 (2021). https://doi.org/10.1016/j.anucene.2021.108596
16. Z.M. Niu, H.Z. Liang, Nuclear mass predictions based on Bayesian neural network approach with pairing and shell effects. Phys. Lett. B **778**, 48–53 (2018). https://doi.org/10.1016/j.physletb.2018.01.002
17. Z.M. Niu, J.Y. Fang, Y.F. Niu, Comparative study of radial basis function and Bayesian neural network approaches in nuclear mass predictions. Phys. Lett. B **100**, 054311 (2019). https://doi.org/10.1103/PhysRevC.100.054311
18. Z.M. Niu, H.Z. Liang, B.H. Sun et al., Predictions of nuclear β -decay half-lives with machine learning and their impact on γ -process nucleosynthesis. Phys. Rev. C **99**, 064307 (2019). https://doi.org/10.1103/PhysRevC.99.064307
19. Z.M. Niu, H.Z. Liang, Nuclear mass predictions with machine learning reaching the accuracy required by γ process studies. Phys. Rev. C **106**, L021303 (2022). https://doi.org/10.1103/PhysRevC.106.L021303
20. Y.G. Ma, L.G. Pang, R. Wang et al., Phase transition study meets machine learning. Chin. Phys. Lett. **40**, 122101 (2023). https://doi.org/10.1088/0256-307X/40/12/122101
21. W.B. He, Q.F. Li, Y.G. Ma et al., Machine learning in nuclear physics at low and intermediate energies. Sci. China Phys. Mech. Astro. **66**, 282001 (2023). https://doi.org/10.1007/s11433-023-2116-0
22. Q.K. Sun, Y. Zhang, Z.R. Hao et al., Enhancing reliability in photo nuclear cross-section ftting with Bayesian neural networks. Nucl. Sci. Tech. **36**, 52 (2025). https://doi.org/10.1007/s41365-024-01611-1
23. C.W. Ma, D. Peng, H.L. Wei et al., Isotopic cross-sections in proton induced spallation reactions based on the Bayesian neural network method. Chin. Phys. C **44**, 014104 (2020). https://doi.org/10.1088/1674-1137/44/1/014104
24. C.W. Ma, D. Peng, H.L. Wei et al., A Bayesian-neural-network prediction for fragment production in proton induced spallation reaction. Chin. Phys. C **44**, 124107 (2020). https://doi.org/10.1088/1674-1137/abb657
25. D. Peng, H.L. Wei, X.X. Chen et al., Bayesian evaluation of residual production cross sections in proton-induced nuclear spallation reactions. J. Phys. G Nucl. Part. Phys. **49**, 085102 (2022). https://doi.org/10.1088/1361-6471/ac7069
26. C.W. Ma, H.L. Wei, X.Q. Liu et al., Nuclear fragments in projectile fragmentation reactions. Prog. Part. Nucl. Phys. **121**, 103911 (2021). https://doi.org/10.1016/j.ppnp.2021.103911
27. X.B. Wei, H.L. Wei, C.W. Ma et al., Predictions from several models for the cross sections of light neutron-rich isotopes by Q_g systematics in ^{40}Ar projectile-fragmentation reactions. Phys. Rev. C **111**, 034607 (2025). https://doi.org/10.1103/PhysRevC.111.034607
28. C.W. Ma, X.B. Wei, X.X. Chen et al., Precise machine learning models for fragment production in projectile fragmentation reactions using Bayesian neural networks. Chin. Phys. C **46**, 7 (2022). https://doi.org/10.1088/1674-1137/ac5efb
29. X.B. Wei, H.L. Wei, Y.T. Wang et al., Multiple-models predictions for drip line nuclides in projectile fragmentation of ^{40,48}Ca, ^{58,64}Ni, and ^{78,86}Kr at 140 MeV/u. Nucl. Sci. Tech. **33**, 155 (2022). https://doi.org/10.1007/s41365-022-01137-4
30. C.W. Ma, X.X. Chen, X.B. Wei et al., Systematic behavior of fragments in Bayesian neural network models for projectile fragmentation reactions. Phys. Rev. C **108**, 044606 (2023). https://doi.org/10.1103/PhysRevC.108.044606
31. J.C. Pei, Recent progress in microscopic nuclear fission dynamics. Chin. Sci. Bull. (in Chinese) **68**, 1066–1073 (2023). https://doi.org/10.1360/TB-2022-1090
32. C.Y. Qiao, J.C. Pei, Z.A. Wang et al., Bayesian evaluation of charge yields of fission fragments of ^{239}U. Phys. Rev. C **103**, 034621 (2021). https://doi.org/10.1103/PhysRevC.103.034621
33. C.Y. Qiao, J.C. Pei, Z.A. Wang et al., Study of energy dependence of neutron induced fission yield ^{235}U with Bayesian machine learning (in Chinese). Atomic Energy Science and Technology **56**, 937–943 (2022). https://doi.org/10.7538/yzk.2022.youxian.0198
34. Y. Qiang, J.C. Pei, K. Godbey, Quantum entanglement in nuclear fission. Phys. Lett. B **861**, 139248 (2025). https://doi.org/10.1016/j.physletb.2025.139248
35. Z.A. Wang, J.C. Pei, Y. Liu et al., Bayesian evaluation of incomplete fission yields. Phys. Rev. Lett. **123**, 122501 (2019). https://doi.org/10.1103/PhysRevLett.123.122501

36. U. Brosa, Multimodal fission and neutron evaporation. Phys. Rev. C **38**, 1944 (1988). https://doi.org/10.1103/PhysRevC.38.1944
37. U. Brosa, S. Grossmann, A. Müller et al., Nuclear scission. Phy. Rep. **4**, 167–262 (1990). https://doi.org/10.1016/0370-1573(90)90114-H
38. N.A. Demekhina, G.S. Karapetyan, Symmetric and asymmetric modes of ^{232}Th photofission at intermediate energies. Phys. At. Nucl. **73**, 24–33 (2010). https://doi.org/10.1134/S1063778810010047
39. P. Moller, Odd-multipole shape distortions and the fission barriers of elements in the region $84 \le z \le 120$. Nucl. Phys. A **192**, 3 (1972). https://doi.org/10.1016/0375-9474(72)90090-5
40. K.H. Schmidt, S. Steinhäuser, C. Böckstiegel et al., Relativistic radioactive beams: a new access to nuclear-fission studies. Nucl. Phys. A **665**, 3 (2000). https://doi.org/10.1016/S0375-9474(99)00384-X
41. K.H. Schmidt, B. Jurado, C. Amouroux et al., General description of fission observables: GEF model code. Nucl. Data Sheets **131**, 107 (2016). https://doi.org/10.1016/j.nds.2015.12.009
42. A. Chatillon, J. Taïeb, H. Alvarez-Pol et al., Experimental study of nuclear fission along the thorium isotopic chain: from asymmetric to symmetric fission. Phys. Rev. C **99**, 054628 (2019). https://doi.org/10.1103/PhysRevC.99.054628
43. J.F. Martin, J. Taieb, A. Chatillon et al., Studies on fission with ALADIN. Eur. Phys. J. A **51**, 174 (2015). https://doi.org/10.1140/epja/i2015-15174-0
44. J.L. Rodríguez-Sánchez, J. Benlliure, J. Taieb et al., Complete characterization of the fission fragments produced in reactions induced by ^{208}Pb projectiles on proton at 500 MeV. Phys. Rev. C **91**, 064616 (2015). https://doi.org/10.1103/PhysRevC.91.064616
45. E. Pellereau, J. Taieb, A. Chatillon et al., Accurate isotopic fission yields of electromagnetically induced fission of ^{238}U measured in inverse kinematics at relativistic energies. Phys. Rev. C **95**, 054603 (2017). https://doi.org/10.1103/PhysRevC.95.054603
46. A. Chatillon, J. Taïeb, H. Alvarez-Pol et al., Evidence for a new compact symmetric fission mode in light Thorium isotopes. Phys. Rev. Lett. **124**, 202502 (2020). https://doi.org/10.1103/PhysRevLett.124.202502
47. J.C. Hogan, A.E. Richardson, J.L. Meason et al., Photofission of ^{232}Th with 9, 15, and 38 MeV peak bremsstrahlung. Phys. Rev. C **16**, 2296 (1977). https://doi.org/10.1103/PhysRevC.16.2296
48. A. Chattopadhyay, K.A. Dost, I. Krajbich, Mass-yield distributions in photofission of ^{232}Th and ^{238}U. J. Inorganic Nucl. Chem. **35**, 8 (1977). https://doi.org/10.1016/0022-1902(73)80491-9
49. H. Naik, V.T. Nimje, D. Raj et al., Mass distribution in the bremsstrahlung-induced fission of ^{232}Th, ^{238}U and ^{240}Pu. Nucl. Phys. A **853**, 1–25 (2011). https://doi.org/10.1016/j.nuclphysa.2011.01.009
50. H. Naik, A. Goswami, G.N. Kim et al., Mass-yield distributions of fission products from photofission of ^{232}Th induced by 45- and 80-MeV bremsstrahlung. Phys. Rev. C **86**, 054607 (2012). https://doi.org/10.1103/PhysRevC.86.054607
51. H. Naik, T.N. Nathaniel, A. Goswami et al., Mass distribution in the 50-, 60-, and 70-MeV bremsstrahlung-induced fission of ^{232}Th. Phys. Rev. C **85**, 024623 (2012). https://doi.org/10.1103/PhysRevC.85.024623
52. H. Naik, B.S. Shivashankar, H.G. Raj Prakash et al., Measurements of fission yield in 8 MeV bremsstrahlung induced fission of ^{232}Th and ^{238}U. J. Radioanal. Nucl. Chem. **299**, 127–137 (2014). https://doi.org/10.1007/s10967-013-2719-0
53. H. Naik, G.N. Kim, R. Schwengner et al., Fission product yield distribution in the 12, 14, and 16 MeV bremsstrahlung-induced fission of ^{232}Th. Eur. Phys. J. A **51**, 150 (2015). https://doi.org/10.1140/epja/i2015-15150-8
54. H. Naik, G.N. Kim, K. Kim, Mass-yield distributions of fission products in bremsstrahlung-induced fission of ^{232}Th. Phys. Rev. C **97**, 014614 (2018). https://doi.org/10.1103/PhysRevC.97.014614
55. W. Günther, K. Huber, U. Kneissl et al., Symmetric and asymmetric yields in the photofission of^{232}Th, ^{235}U, ^{238}U and ^{239}Pu. Zeitschrift für Physik A Atoms and Nuclei **295**, 333–340 (1980). https://doi.org/10.1007/BF01412945
56. J. Randrup, P. Moller, Energy dependence of fission-fragment mass distributions from strongly damped shape evolution. Phys. Rev. C **88**, 064606 (2013). https://doi.org/10.1103/PhysRevC.88.064606
57. K.X. Jing, Z. Li, C.G. Liu et al., Fission yields in 7.64 MeV gamma induced fission of ^{232}Th. Chin. J. Nucl. Phys. **10**, 244 (1988).
58. O.O. Parlag, V.T. Maslyuk, E.V. Oleynikov et al., Asymmetric modes of photofission fragments mass distribution of Th-232. Naukovyi Visnyk. Uzhgorods kogo Univ. Ser.Fiz., **49**, 54 (2021). https://dspace.uzhnu.edu.ua/jspui/handle/lib/39881
59. Krishichayan, M. Bhike, A.P. Tonchev et al., Fission product yield measurements using monoenergeticphoton beams. EPJ Web Conf. **146**, 04018 (2017). https://doi.org/10.1051/epjconf/201714604018
60. S.W. Krishichayan, C.R. Finch, Howell, et al., Monoenergetic photon-induced fission cross-section ratio measurements for ^{235}U, ^{238}U, and ^{239}Pu from 9.0 to 1.70 MeV. Phys. Rev. C **98**, 014608 (2018). https://doi.org/10.1103/PhysRevC.98.014608
61. Krishichayan, M. Bhike, C.R. Howell et al., Fission product yield measurements using monoenergeticphoton beams. Phys. Rev. C**100**, 014608 (2019).https://doi.org/10.1103/PhysRevC.100.014608
62. J.F. Martin, J. Taleb, G. Boutoux et al., Fission-fragment yields and prompt-neutron multiplicity for Coulomb-induced fission of ^{234,235}U and ^{237,238}Np. Phys. Rev. C **104**, 044602 (2021). https://doi.org/10.1103/PhysRevC.104.044602
63. D. Choudhury, D.L. Balabanski, A. Krasznahorkay et al., High-resolution photofission studies with the gamma beam system at ELI-NP. AIP Conf. Proc. **1852**, 070003 (2017). https://doi.org/10.1063/1.4984873
64. P. Constantin, D.L. Balabanski, P.V. Cuong et al., Simulation of photofission experiments at the ELI-NP facility. Nucl. Instrum. Meth. A **372**, 78–85 (2016). https://doi.org/10.1016/j.nimb.2016.02.004
65. S. Gales, D.L. Balabanski, F. Negoita et al., New frontiers in nuclear physics with high power lasers and brilliant monochromatic gamma beams. Phys. Scr. **91**, 093004 (2016). https://doi.org/10.1088/0031-8949/91/9/093004
66. H.W. Wang, G.T. Fan, H.H. Xu et al., Construction and trial operation of Shanghai laser electron gamma source. Nucl. Phys. Rev. **(in Chinese) 41**, 67–74 (2024). https://doi.org/10.11804/NuclPhysRev.41.2023CNPC38)
67. R.Z. Tai, Z.T. Zhao, Overview of SSRF phase-II beamlines. Nucl. Sci. Tech. **35**, 137 (2024). https://doi.org/10.1007/s41365-024-01487-1